Acta Biomaterialia xxx (xxxx) xxx

Contents lists available at ScienceDirect

Acta Biomaterialia

journal homepage: www.elsevier.com/locate/actbio

Full length article

A microfluidics-based method for culturing osteoblasts on biomimetic hydroxyapatite

Abdul Raouf Atif[a], Michael Pujari-Palmer[b], Maria Tenje[a], Gemma Mestres[a,*]

[a] Division of Microsystems Technology, Department of Materials Science and Engineering, Science for Life Laboratory, Uppsala University, 751 22 Uppsala, Sweden
[b] Division of Applied Materials Science, Department of Materials Science and Engineering, Uppsala University, 751 22 Uppsala, Sweden

ARTICLE INFO

Article history:
Received 3 November 2020
Revised 2 March 2021
Accepted 22 March 2021
Available online xxx

Keywords:
Calcium phosphate cement
Flow
In vitro
On-chip
Shear stress

ABSTRACT

The reliability of conventional cell culture studies to evaluate biomaterials is often questioned, as *in vitro* outcomes may contradict results obtained through *in vivo* assays. Microfluidics technology has the potential to reproduce complex physiological conditions by allowing for fine control of microscale features such as cell confinement and flow rate. Having a continuous flow during cell culture is especially advantageous for bioactive biomaterials such as calcium-deficient hydroxyapatite (HA), which may otherwise alter medium composition and jeopardize cell viability, potentially producing false negative results *in vitro*. In this work, HA was integrated into a microfluidics-based platform (HA-on-chip) and the effect of varied flow rates (2, 8 and 14 µl/min, corresponding to 0.002, 0.008 and 0.014 dyn/cm^2, respectively) was evaluated. A HA sample placed in a well plate (HA-static) was included as a control. While substantial calcium depletion and phosphate release occurred in static conditions, the concentration of ions in HA-on-chip samples remained similar to those of fresh medium, particularly at higher flow rates. Pre-osteoblast-like cells (MC3T3-E1) exhibited a significantly higher degree of proliferation on HA-on-chip (8 μl/min flow rate) as compared to HA-static. However, cell differentiation, analysed by alkaline phosphatase (ALP) activity, showed low values in both conditions. This study indicates that cells respond differently when cultured on HA under flow compared to static conditions, which indicates the need for more physiologically relevant methods to increase the predictive value of *in vitro* studies used to evaluate biomaterials.

Statement of significance

There is a lack of correlation between the results obtained when testing some biomaterials under cell culture as opposed to animal models. To address this issue, a cell culture method with slightly enhanced physiological relevance was developed by incorporating a biomaterial, known to regenerate bone, inside of a microfluidic platform that enabled a continuous supply of cell culture medium. Since the utilized biomaterial interacts with surrounding ions, the perfusion of medium allowed for shielding of these changes similarly as would happen in the body. The experimental outcomes observed in the dynamic platform were different than those obtained with standard static cell culture systems, proving the key role of the platform in the assessment of biomaterials.

1. Introduction

The biomaterials field is steadily growing, with new and modified biomaterial formulations designed to meet the demands of a rapidly aging population. While biomaterials are usually classified in terms of their origin (natural or synthetic) and their chemical nature (*i.e.* ceramic, metal or polymer), there are several physical properties (*e.g.* roughness and porosity) that also play a crucial role in the biological response of biomaterials [1,2]. For this reason, before any newly developed or modified biomaterial is authorized for use in patients, a thorough evaluation of its biocompatibility is required. First, cell culture assays (*in vitro* studies) are per-

* Corresponding author at: Department of Materials Science and Engineering, Uppsala University, Box 35, 751 03 Uppsala, Sweden.
E-mail address: gemma.mestres@angstrom.uu.se (G. Mestres).

https://doi.org/10.1016/j.actbio.2021.03.046
1742-7061/

formed by growing cells on/in the biomaterial. If promising results are obtained, the materials may be implanted in animal models (*in vivo* studies). However, an alarmingly low degree of correlation between conventional *in vitro* and *in vivo* studies has been reported [3]. This means that a biomaterial may enable adequate cell adhesion and proliferation *in vitro*, while failing to do the same *in vivo*, and vice versa. This poor correlation can be ascribed to the complexity of *in vivo* tissues, which entail continuous flow, mechanical load and elaborated cross-talk between cells, with none of these conditions being mimicked in standard cell cultures [4]. Suffice to say, this disconnect between *in vitro* and *in vivo* outcomes leads to time delays, inflated expenditure and excessive usage of animal testing to characterise biomaterials. Improved cell culture models are needed to produce results that are predictive of the real outcomes of implanting a biomaterial in the body [3,4].

A biomaterial showing a low correlation between *in vitro* and *in vivo* studies is calcium-deficient hydroxyapatite (HA). Although HA displays excellent biocompatibility *in vivo* [5], its bioactive properties may compromise cell viability if the culture is done under static conditions [6–8]. In particular, it has been reported that HA can uptake calcium ions from and release phosphate ions into the environment [6,7,9], thereby influencing osteoblast proliferation and differentiation *in vitro* [7,10]. For this reason, alternative culture methods that provide flow, as inspired by the dynamic interstitial fluid flow [11,12], are appealing to evaluate the biological properties of HA.

The bone microenvironment is highly ordered and regulated by mechanosensitive mechanisms, where application of mechanical load increases bone anabolism in the affected area [13]. Specifically within the bone, osteocytes transduce the shear stress of the interstitial fluid within the lacuno-canalicular network (LCN) into molecular signals that stimulate osteoblasts to synthesize new bone tissue [14]. Briefly, the load applied on the bone during movement causes the compression of the interstitial fluid within the LCN, forcing its extravasation towards the Haversian canal located in the centre of the osteon [14]. Due to the narrowness of the canaliculi, this transient flow imparts considerable shear stimulation on the osteocytes located within the LCN, thus stimulating biological responses [15]. By applying flow during *in vitro* testing, which in turn causes shear stress, this aspect of bone physiology may be partially recreated, leading to differing cell responses as compared to static cultures [16–19].

Nowadays, there exists a large gap between the physiology of bone and the common *in vitro* tests used to evaluate biomaterials. Typical *in vitro* tests consist of culturing cells on the surface of a biomaterial maintained in a well plate, replacing the culture medium manually several times a week [20]. Albeit less frequent, cell culture on/in a biomaterial can be done in bioreactors, which allow for a continuous movement of culture medium either on the biomaterial surface or through a macroporous biomaterial with interconnected pores. Although bioreactors better replicate physiological features such as shear stress [21], they require experienced operators and a large amount of cells and culture medium. These drawbacks can potentially be overcome by microfluidic technology.

Microfluidics technology involves precise control of microliter-sized fluid volumes, enabling the manipulation of fluid composition and shear stress. It therefore provides new possibilities to precisely stimulate cells within a confined channel, enabling potential to imitate the microenvironment of a tissue [4]. For example, flow control can be used to reasonably mimic the nutrient-provision and waste-removal effects of the blood vasculature. Only recently, microfluidics has been explored as a tool to evaluate the biological properties of biomaterials [4,22–27]. Of special interest is the work performed by Tang et al., who used a photo-patterned and sintered HA to fabricate microfluidic chips, and created concentration gradients with a model drug [28].

The aim of this work was to integrate HA in a microfluidic platform and to assess the behaviour of pre-osteoblast-like MC3T3-E1 cells cultured in this microenvironment. The continuous medium supply provided by the microfluidic HA-platform was expected to alleviate changes in calcium and phosphate concentrations in the culture medium and provide nutrients to cultured cells. A specific flow rate, adequate in terms of ionic concentration shielding and concomitant cell growth was selected, and then biochemical assays were performed to evaluate cell proliferation and differentiation.

2. Materials and methods

2.1. Fabrication of biomimetic hydroxyapatite (HA) and HA-on-chip

2.1.1. Biomimetic hydroxyapatite (HA)

Biomimetic calcium-deficient hydroxyapatite (HA) was prepared through a cementitious reaction. Alpha-tricalcium phosphate (α-TCP, $Ca_3(PO_4)_2$) was used as the solid phase of the cement. HA was synthesized by mixing dicalcium phosphate anhydrous ($CaHPO_4$, #40232.30, Alfa Aesar) and calcium carbonate ($CaCO_3$, #10687192, Acros Organics) in a 2:1 molar ratio. The mixture was heated on a zirconia setter plate at 1450 °C for 5 h (total thermal treatment of 18 h), in an Entech MF 4/16 furnace and quenched in air. Afterwards, the powder was dry milled in a planetary ball mill (PM 400, Retsch) in a 500 ml zirconia-milling jar, at 300 rpm for 15 min, with 100 g per 100 zirconia-milling balls (10 mm diameter). The purity of α-TCP was verified by X-ray diffraction and its particle size distribution evaluated by laser diffraction. As the liquid phase, 2.5 w/v% sodium phosphate dibasic (Na_2HPO_4, #S7907, Merck) in ultrapure water was prepared. Calcium phosphate cement (CPC) was prepared by mixing the solid phase and the liquid phase in a liquid-to-powder ratio of 0.65 ml/g.

The CPC paste was shaped in Teflon moulds (ø = 6 mm, h = 2 mm or ø = 15 mm, h = 2 mm). The discs (after setting at 37 °C in 100% relative humidity for 4 h to ensure cohesion) were immersed in a 0.9 w/v% sodium chloride (NaCl, #S7653, Merck) solution at 37 °C for 10 days for full transformation into biomimetic HA. The setting time of the cement as well as the characterisation of the HA, including morphology by scanning electron microscopy, crystalline phases by X-ray diffraction and compressive strength by a universal testing machine are described in the Supplementary Material section (Table S.M. 1, Figs. S.M. 1, S.M. 2 and S.M. 3).

2.1.2. HA-on-chip

Microfluidic chips based on polydimethylsiloxane (PDMS) and glass were developed to integrate HA as a substrate of a microchannel. PDMS (Sylgard 184, Dow Corning) base elastomer was mixed with the corresponding curing agent in a 10:1 ratio. PDMS moulds were replicated by soft lithography from additive manufactured moulds (RS-F2-GPBK-04 black resin, Formlabs) and cured at 60 °C for 2 h.

The CPC paste was introduced into a PDMS mould containing three rectangular pockets (l = 18 mm, w = 3 mm, h = 0.8 mm), set for 4 h at 37 °C and 100% humidity conditions and then immersed in a 0.9 w/v% NaCl solution at 37 °C for 10 days to allow for transformation into HA. After this time had elapsed, the HA rods were carefully removed from the first mould and fit into another PDMS mould with deeper cavities (l = 18 mm, w = 3 mm, h = 1.3 mm), leaving a channel height of 0.5 mm. In the latter moulds, the end sides of the rectangular cavity were extended into a triangular semi-circle (ø = 2 mm) to decrease the risk of bubble formation by avoiding a drastic change in geometry (Fig. 1A).

The HA-side surface of the PDMS piece and a glass slide with six drilled holes (ø = 0.8 mm) were plasma treated (Atto plasma

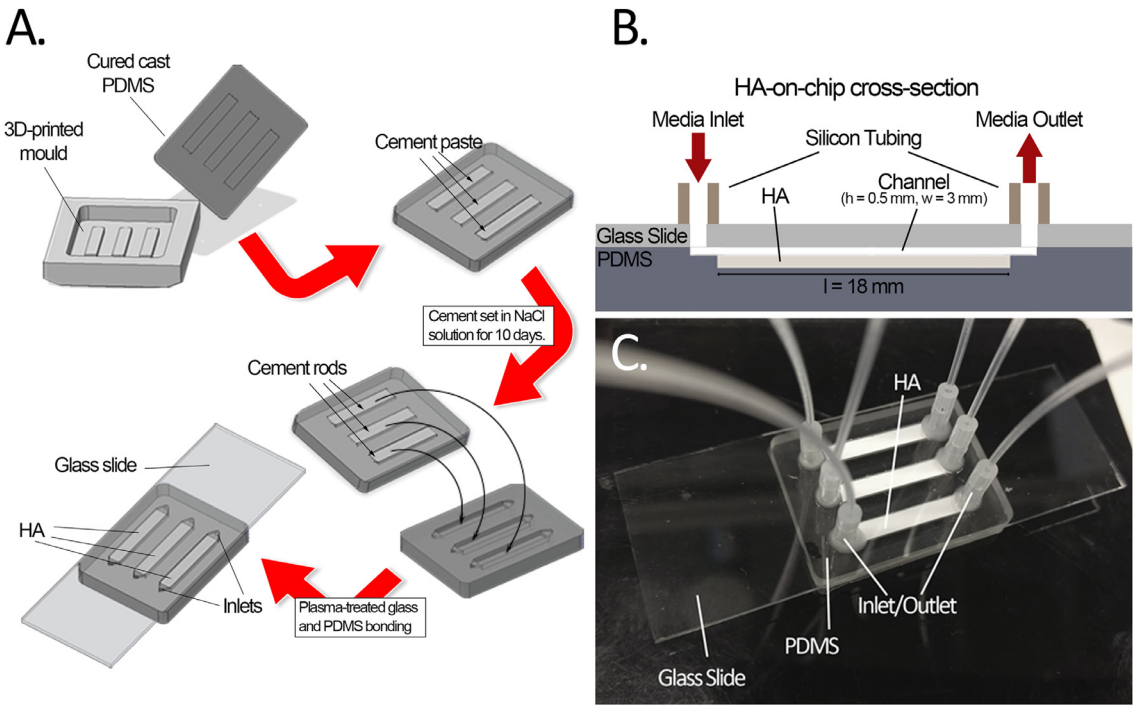

Fig. 1. A) Steps involved in the fabrication process of HA-on-chip, B) schematic cross-section of the HA-on-chip and C) photograph of a HA-on-chip.

oven, Diener electronic GmbH) for 1 min (40 kHz, 200 W) in air and subsequently bonded together, aligning the holes to the PDMS channels (Fig. 1A). Short tubing pieces (#228-0701, VWR International) were glued (Elastosil A07 Adhesive, Wacker Chemie AG) to the drilled holes on the glass slides to serve as fittings for the inlet/outlet tubing (#427405, BD). This platform, HA-on-chip, comprised HA embedded in three separate channels to allow for triplicate analysis. The cross-section of HA-on-chip is displayed in Fig. 1B and the constructed chip is shown in Fig. 1C.

2.1.3. Ionic exchange between HA and cell culture medium

The ionic exchange experienced by cell culture medium in contact with HA was monitored under dynamic and static conditions. The medium was prepared by supplementing Minimum Essential Medium Alpha (MEM α, Hyclone, #SH3026501) with 10 mg/ml bovine serum albumin (BSA, #A9418, Merck) to produce a simplified protein-containing medium. A total volume of 1 ml of medium was perfused through HA-on-chip for each different flow rate condition (2, 8 and 14 µl/min) using a syringe pump (PHD-2000 infusion, Harvard Apparatus). The static condition was assessed by immersing a HA disc (ø = 15 mm, h = 2 mm) in 1 ml of MEM in a 24 well plate for 24 h. Fresh medium was used as control. The samples were analysed using ICP-OES (Avio 200 ICP Optical Emission Spectrometer, Perkin-Elmer) to quantify the atomic concentrations of calcium ($[Ca^{2+}]$) and phosphorus ($[P^{5+}]$), the latter of which enabled indirect quantification of inorganic phosphate in the medium. The experiment was performed twice, with duplicates taken for all samples, except HA-static, where triplicates were taken.

Prior to the ICP-OES analysis, the samples were filtered using 0.2 µm polyethersulfone (PES) syringe filters (#6782-1302, Whatman) and diluted in 2 v/v% nitric acid (HNO_3, #100456, Merck). As calibration standards, 50 µg/ml Ca (#N9300108, Perkin-Elmer) and 1000 µg/ml P (#N9300139, Perkin-Elmer) solutions were used. The samples were introduced to the system using a flow rate of 1 ml/min and a set delay time of 30 s between each sample.

2.2. Cell culture studies

2.2.1. Cell culture conditions

MC3T3-E1 mouse pre-osteoblast-like cells (subclone 14, ATCC) were utilized as they are a well-established model of osteoblast biology [29]. The cells were maintained in ascorbic acid-free MEM α (Gibco, #A1049001, Thermo Fischer Scientific), which was supplemented with 10 v/v% of Fetal Bovine Serum (FBS Hyclone, #SV3016003, GE Healthcare) and 1 v/v% Penicillin/Streptomycin (#DE17-602E, BioWhittaker). Ascorbic acid-free MEM α was used when maintaining the cells to avoid any stimulation towards cell differentiation [30]. The medium was changed every third day and the cells were trypsinized and split before a confluence of 80% was reached. For cell cultures used in experimental runs, Hyclone MEM α supplemented with 10 v/v% FBS and 1 v/v% penicillin/streptomycin was used. This medium will be referred to as supplemented medium in the text. Cell cultures were maintained in a cell incubator (Heracell 150) with a controlled internal humidified environment of 37 °C and 5% of CO_2.

2.2.2. Cell viability at different flow rates

Cells were cultured in HA-on-chip under dynamic (2, 8 and 14 μl/min) and static (termed HA-on-chip-static) conditions. Cells were also grown on two materials in static conditions: HA discs (ø = 6 mm) placed in 96 well plates (termed as HA-static) and directly on the polystyrene substrate (PS) of 96 well plates (termed PS-static).

Prior to cell culture studies, HA-on-chip and HA discs were sterilized with 70% ethanol for 2 h. Afterwards, the ethanol was removed by extensive rinsing in autoclaved distilled water and the materials were pre-incubated overnight in supplemented medium (with flow at 1 µl/min in the case of HA-on-chip).

50,000 cells/cm^2 were seeded on the surface of HA-on-chip (both under flow and static samples), HA-static and PS-static. Specifically, in the case of the HA-on-chip, cells were seeded at a cell density of 900,000 cells/ml using a volume of 30.5 µl. In the case of HA-static and PS-static samples, cells were seeded

Table 1
Shear stresses and flow velocities of the three flow conditions.

	Flow rate (µl/min)		
	2	8	14
Shear stress (dyn/cm^2)	0.002	0.008	0.014
Flow velocity (µm/s)	22.2	88.9	155.6

at 70,700 and 120,000 cells/ml, respectively, using a volume of 200 µl. Cells were allowed to attach, undisturbed, for 2 h in HA-on-chip samples as preliminary studies had indicated it to be enough time to ensure sufficient cell adhesion on the material's surface (Fig. S.M. 4). Afterwards, a peristaltic pump (LabV1-II, Shenchen) connected to dynamic HA-on-chip samples was started and maintained continuously at a flow rate of 2, 8 or 14 µl/min. A peristaltic pump was used as it allowed for larger medium reservoirs, enabling long-term cell culture. Eqs. (1) and (2) indicate wall shear stress and flow velocity calculations, respectively, and the corresponding values are shown in Table 1. The HA-on-chip-static samples were kept in closed Petri dishes and an excess of supplemented medium was added in PDMS reservoirs bonded on the inlets and outlets to reduce the effects of evaporation. The supplemented medium in the HA-on-chip-static, HA-static and PS-static was replaced daily. The experiments were performed with triplicates for each sample.

$$\text{Wall shear stress}: \tau = \frac{6\eta Q}{h^2 w} \quad (1)$$

$$\text{Flow velocity}: \ u = Q/A \quad (2)$$

where τ is wall shear stress, η is viscosity (0.748 cP [31]), Q is flow rate, h is channel height, w is channel width, u is flow velocity and A is cross-sectional area.

Cell viability was evaluated by imaging at 6 and 72 h. The samples were rinsed twice in phosphate-buffered saline (PBS), stained with calcein (1 µg/ml, #C3099, Thermo Fisher Scientific), propidium iodide (0.67 µg/ml, #P3566, Thermo Fisher Scientific) and Hoechst 33342 (5 µg/ml, #62249, Thermo Fisher Scientific), and afterwards incubated for 25 min at 37 °C. Cells were imaged using a fluorescent microscope (IX73 Inverted Microscope, Olympus, Tokyo, Japan). Cell count averages were obtained from multiple representative images, which were methodically taken at three to five different locations on each sample, using triplicate samples. The background of HA-on-chip and HA-static images was reduced using rolling ball background subtraction, with a rolling ball radius of 1000 pixels using Fiji (ImageJ 1.52 g) software [32]. Finally, the imaged calcein-stained cells were manually counted with the aid of Fiji software [32].

2.2.3. Cell proliferation and differentiation

Due to appreciable ionic exchange shielding (Fig. 2) and good cell viability (Fig. 3), a flow rate of 8 µl/min was selected to evaluate cell proliferation and differentiation over 10 days. 50,000 cells/cm^2 were seeded in supplemented medium on HA-on-chip, HA-static and PS-static samples. Cell proliferation, differentiation and imaging (calcein, propidium iodide and Hoechst stains) were evaluated at 1, 5 and 10 days of culture. In addition, calcium and phosphorous atomic concentrations were measured via ICP-OES every 24 h from culture medium that perfused out of the HA-on-chip, as well as supernatant medium from the static samples (HA-static and PS-static). The experiment was performed twice, with triplicate samples per condition in each experiment.

Cell proliferation was indirectly evaluated via the use of a Lactate Dehydrogenase (LDH) assay. Cytosolic LDH activity allowed quantification of viable cells adhered on the samples prior to cell lysis. Cell differentiation was evaluated by quantification of alkaline phosphatase (ALP) enzymatic activity, which is expressed as an early stage marker of osteoblast differentiation. Prior to the biochemical assays, the samples were rinsed with PBS to remove cells that were not adhered to the material. The HA-on-chip was disconnected from the tubing before lysis buffer was added using a pipette. Afterwards, 40 µl and 200 µl of 10 v/v% cell lysis buffer solution (TOX-7 LDH kit, Merck) in PBS was added to HA-on-chip and static samples, respectively. The samples were incubated for 50 min at 37 °C and the lysates were collected. In the case of HA-static, the HA discs were transferred to new wells prior to the addition of lysis buffer to avoid the potential effect of cells that could be growing underneath the disc on the well plate surface. The solution extracted from HA-on-chip was diluted 5-fold in fresh 10 v/v % cell lysis buffer solution to equalise the volume to that of the static samples. In the case of the LDH analysis, all samples were further diluted 5-fold in PBS to avoid signal saturation.

LDH assay was done following the manufacturer's instructions. Briefly, 50 µl of diluted lysed sample was added to 100 µl of LDH assay reagent in a 96-well plate. The plate was incubated at room temperature for 20 min, after which sample and background absorbance were measured at 490 and 690 nm, respectively, using a microplate reader (Spark®, TECAN). A LDH standard curve was performed to transform absorbance values into relative cell number, with the values obtained being normalized against growth area in cm^2.

ALP assay was performed according to the manufacturer's protocol. Briefly, 50 µl of undiluted lysed sample was added to 100 µl of p-nitrophenyl phosphate solution (Alkaline Phosphatase Yellow Liquid Substrate, #P7998, Merck) in a 96-well plate. The plate was incubated at room temperature for 20 min, after which absorbance was measured at 405 nm using a plate reader. A standard curve with known concentrations of p-nitrophenol (#N7660, Sigma-Aldrich) was prepared to transform absorbance values to p-nitrophenol concentration. ALP activity was normalized against cell number obtained from the LDH assay and the reaction time.

2.3. Statistical analysis

All data points were plotted as a mean ± standard deviation of the sample replicates in each experiment. Significance testing was performed via a one-way, two-sided ANOVA analysis with a significance level of $\alpha = 0.05$. Post-hoc Tukey or Dunett's tests were done to investigate significant pair-wise differences and differences against control samples, respectively. All statistical analysis was performed in Minitab17.

3. Results

3.1. Ionic interaction of HA-on-chip at different flow rates

As presented in Fig. 2A, a HA disc immersed in cell culture medium in static conditions for 24 h led to a 47.0 ± 5.1% reduction in [Ca^{2+}] in comparison to fresh medium ($p < 0.0005$). By flowing culture medium through HA-on-chip at three different flow rates (2, 8 and 14 µl/min), the reduction of [Ca^{2+}] was not as pronounced, with a decrease of 35.8 ± 8.2% ($p = 0.001$), 17.5 ± 2.5% ($p = 0.04$) and 7.5 ± 4.5%, respectively, in comparison to fresh medium. As such, [Ca^{2+}] in HA-on-chip were closer to those in fresh medium as flow rate was increased. As shown on Fig. 2B, the same principle applied for [P^{5+}], but with an ionic release instead of a depletion profile. In HA-static, an increase of 96.2 ± 5.5% ($p < 0.0005$) in [P^{5+}] compared to fresh medium was observed. By flowing medium at 2, 8 and 14 µl/min, this difference was less prominent, with [P^{5+}] being 35.4 ± 8.1 % ($p = 0.001$), 9.2 ± 1.9% and 9.0 ± 2.2% higher than fresh medium, respectively.

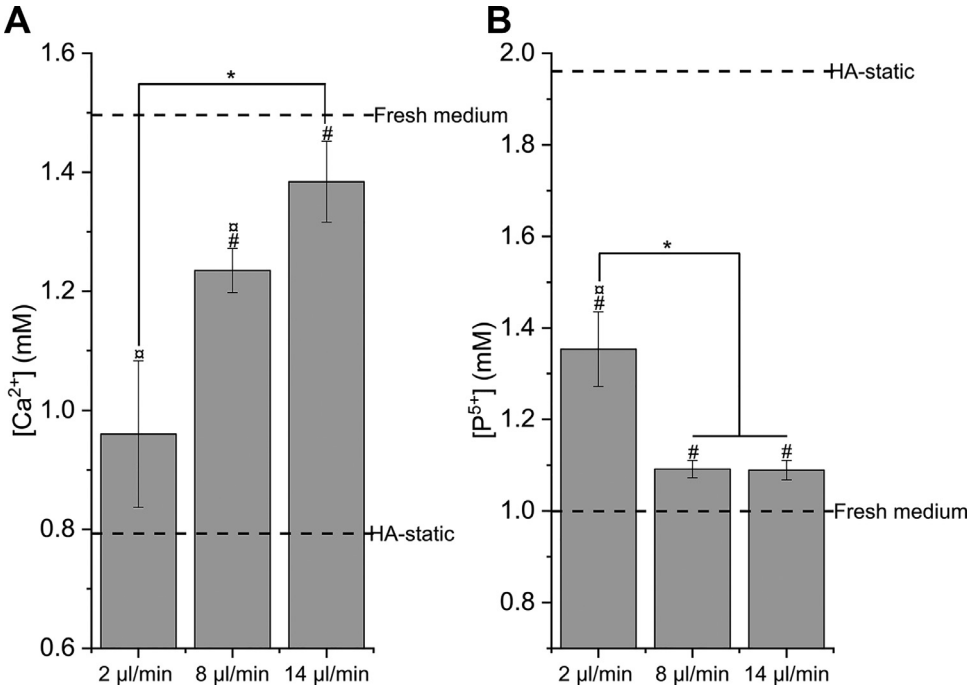

Fig. 2. A) $[Ca^{2+}]$ and B) $[P^{5+}]$ in outgoing cell culture medium flown through HA-on-chip at three different flow rates: 2, 8 and 14 µl/min. Two controls are indicated in dashed lines: HA-static (medium in contact with a HA disc in a well plate for 24 h) and fresh medium. * indicates statistical difference between samples ($p < 0.05$, Post-hoc Tukey test); ¤ indicates statistical difference against fresh medium and # against HA-static ($p < 0.05$, Dunett's test).

3.2. Cell culture studies

3.2.1. Evaluation of cell growth on HA-on-chip at different flow rates

MC3T3-E1 cells were seeded on HA-on-chip samples and maintained under 2, 8 or 14 µl/min flow rates, with cultures imaged after 6 and 72 h. As observed in Fig. 3A, cells adhered on HA-on-chip (under flow), HA-static and PS-static samples after 6 h of culture, but failed to adhere to HA-on-chip-static. After 72 h, cells on HA-on-chip samples showed a substantial increase in cell number at the three flow rates evaluated. According to image quantification (Fig. 3B), the cell count from 6 h to 72 h increased by approximately 2.9-fold in the 2 µl/min sample ($p < 0.0005$), 1.6-fold in the 8 µl/min sample ($p = 0.04$), 2.2-fold in the 14 µl/min sample ($p = 0.003$) and 3.1-fold in PS-static ($p < 0.0005$) in comparison to the respective 6 h samples. In comparison, cell counts in HA-static decreased 0.9-fold between 6 h and 72 h.

3.2.2. Ionic exchange, cell proliferation and differentiation of HA-on-chip

$[Ca^{2+}]$ and $[P^{5+}]$ were evaluated in the culture medium where MC3T3-E1 cells were maintained, both at 8 µl/min and in static conditions, for a 10 day period. The flow of 8 µl/min was picked as it appeared ideal in terms of shielded ionic exchange and favourable cell viability. As shown in Fig. 4A, the HA-on-chip medium displayed a level of $[Ca^{2+}]$ similar to that of fresh medium (1.57 ± 0.03 mM), with $[Ca^{2+}]$ being slightly lower than fresh medium for the first 4 days and slightly higher for days 7–9. On the other hand, there was a rapid decrease in $[Ca^{2+}]$ in HA-static culture medium, which showed values between 0.39 and 0.46 mM from the second day onwards, all of which were statistically lower than that of fresh medium ($p < 0.0005$ for all, Table S.M. 2). As for $[P^{5+}]$ (Fig. 4B), the $[P^{5+}]$ of HA-on-chip medium (values between 0.99 and 1.24 mM) appeared to be statistically lower than that of fresh medium (1.28 ± 0.04 mM) for days 3, 4, 6 and 8 (p values in Table S.M. 3). As for HA-static samples, the medium showed a $[P^{5+}]$ peak on day 2 (2.83 ± 0.08 mM) that was double that of fresh medium ($p < 0.0005$, Table S.M. 3), followed by a gradual decline towards levels in fresh medium along the 10-day experiment.

Proliferation and differentiation were evaluated for MC3T3-E1 cells maintained on HA-on-chip at 8 µl/min, with HA-static and PS-static included as controls. As depicted in Fig. 5A, cells cultured on HA-static failed to proliferate and instead exhibited an initial decline in signal, which remained low over the experimental period. In contrast, cells cultured on HA-on-chip showed a sustained degree of proliferation over the 10-day period. Specifically, the number of cells recorded on the HA-on-chip samples was 1.63-fold, 17.6-fold ($p < 0.0005$) and 24.3-fold ($p < 0.0005$) higher as compared to HA-static on day 1, 5 and 10, respectively. In order to ensure that the cells proliferated as expected, PS-static samples were used as a positive control and showed a consistent degree of proliferation over the experimental period. The live and dead cells of all samples were visualised on day 10. As shown in Fig. 5B, the cell cultures in both HA-on-chip and PS-static samples appeared confluent. This was opposed to cell cultures on HA-static samples, which were far less numerous in comparison.

As illustrated in Fig. 6, cells cultured on HA-on-chip and HA-static displayed no significant increase in ALP expression over the experimental period. Specifically, the ALP activity of cells on HA-on-chip samples was 4.29-fold higher compared to HA-static on day 1, while they were the same on day 5 and 10. At 5 and 10 days of culture, ALP expression was significantly more pronounced by cells cultured on PS-static than by cells cultured on HA-on-chip or HA-static samples, which showed similar levels of ALP expression.

4. Discussion

Calcium-deficient hydroxyapatite (HA) is a bioactive material with a large capacity to uptake ions from culture medium [6,9], which can lead to ionic imbalances that reduce cell viability *in vitro* under static conditions [33,34]. In contrast, HA exhibits ex-

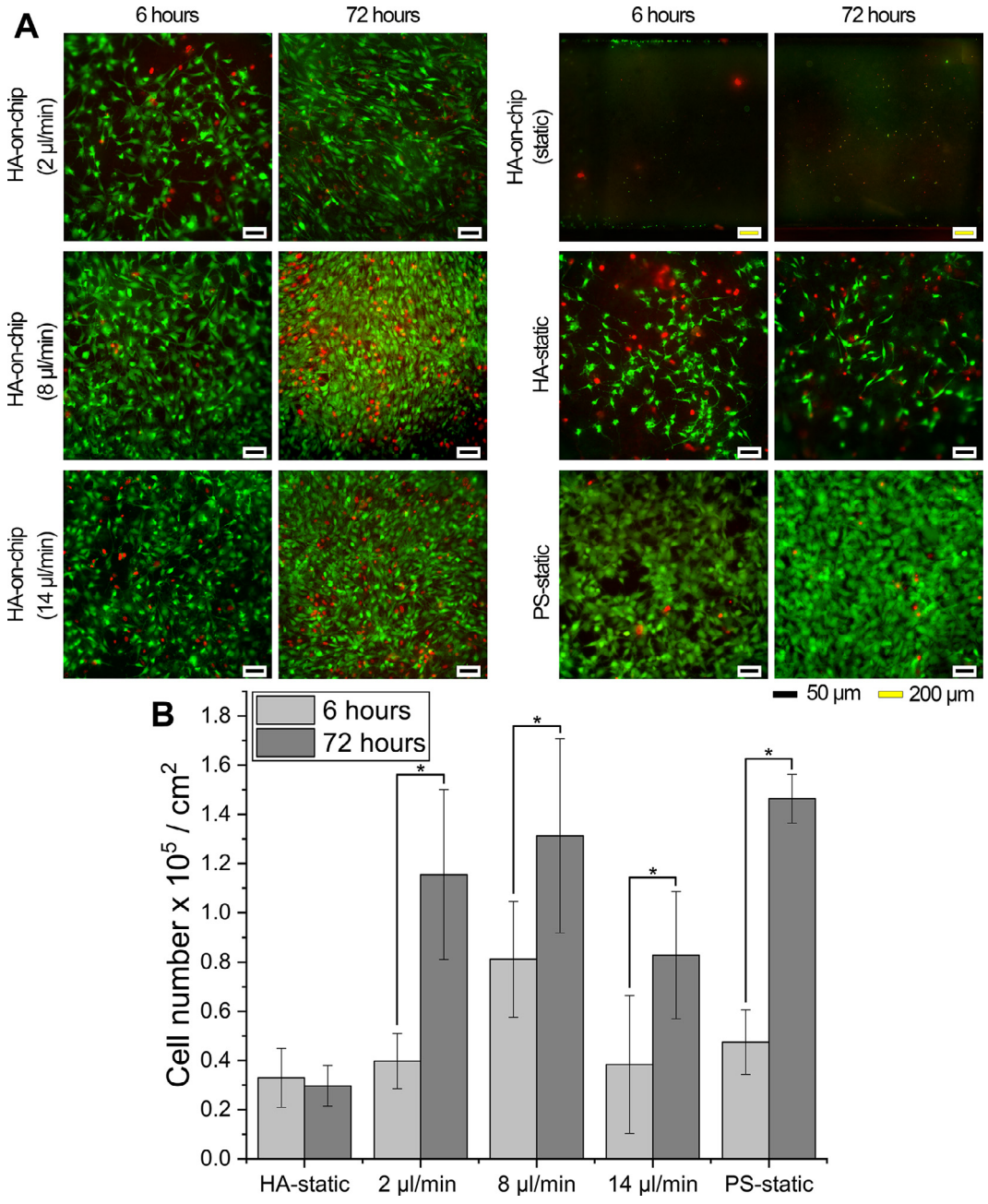

Fig. 3. **A**) MC3T3-E1 cells cultured on HA-on-chip (static, 2, 8 and 14 µl/min), HA-static and PS-static stained with calcein and propidium iodide, at 6 h and 72 h of culture. **B**) Semi-quantification of calcein stained cells. * indicates statistical difference between cell count at 6 h and 72 h for a given sample ($p < 0.05$, Post-hoc Tukey test).

cellent biocompatibility *in vivo* [5], indicating that the circulation of physiological fluids around the biomaterial provides a necessary buffering effect, where depleted ions are rapidly replenished, thus maintaining adequate ionic concentrations in the environment [7,33,35]. An approach to reduce the effects of the ionic exchange of HA in a static cell culture was recently proposed by Sadowska et al., who reduced the size of HA samples and increased the volume of culture medium, resulting in improved cell viability over time [34]. Taking this approach a step further, implementing a continuous flow *in vitro* can be especially advantageous to assessing the biological properties of HA.

Only recently has microfluidics been envisioned as a tool to integrate biomaterials and enable a cell culture environment that more moderately resembles the physiological condition. In such systems, cells can be cultured on the biomaterial in constrained spaces and with a continuous flow in order to modestly replicate the natural packed tissues and the refreshment of the interstitial fluid [4,26,36]. In this work, by developing a microfluidic platform for biomaterial evaluation, we aimed to capitalize on aforementioned advantages of dynamic medium change and shear stress stimulation, which are characteristic of the body tissue and unavailable in standard culturing systems, while also enabling other features such as *in situ* cell imaging [4].

In the current work, when HA was maintained in static culture medium over 10 days, [Ca^{2+}] was continuously depleted and [P^{5+}] was constantly released (Figs. 2 and 4), despite daily changes of the culture medium. This correlated well with a previous study in terms of both magnitude and timing, even capturing the gradual recovery of both ion concentrations towards fresh medium levels (Fig. 4) [6]. This phenomena can be explained by the ca-

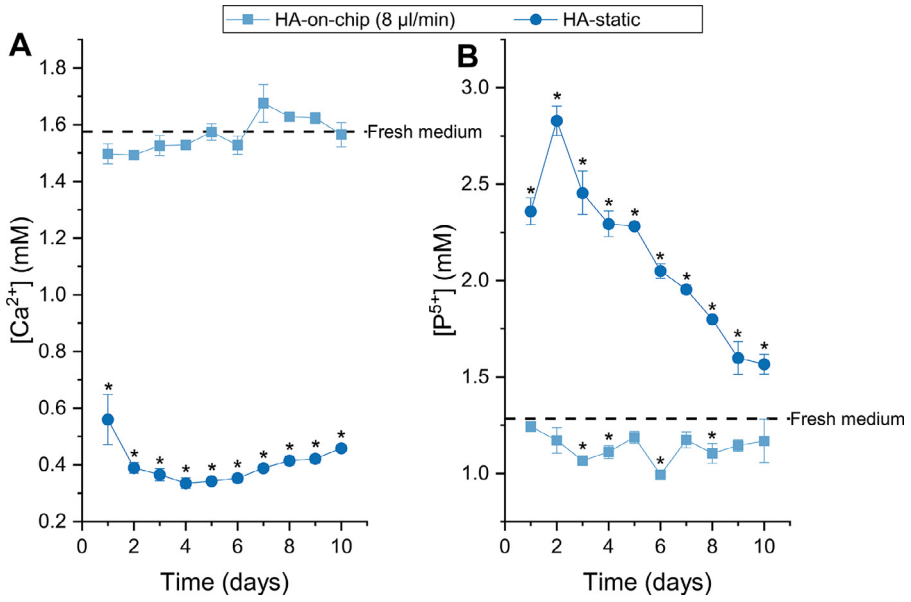

Fig. 4. Quantification of A) $[Ca^{2+}]$ and B) $[P^{5+}]$ in the culture medium of HA-on-chip (8 μl/min) and HA-static over the 10-day period of the cell culture study. The data represents separate values at each collection point, and is not cumulative. * indicates statistical difference between a sample time-point and fresh medium ($p < 0.05$, Dunett's test).

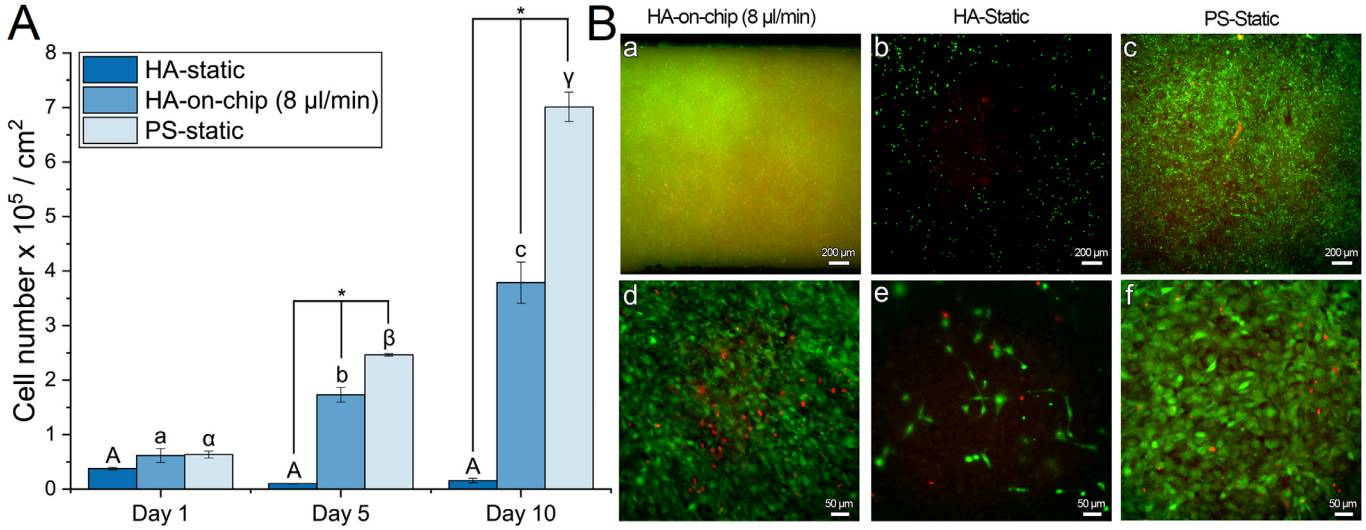

Fig. 5. A) Cell proliferation quantified by LDH assay, with values expressed as cell number per cm^2. Identical letters with the same format indicate no statistical difference between samples of the same type at different time points. * indicates statistical difference between sample types at the same time-point ($p < 0.05$, Post-hoc Tukey test). B) Imaging of MC3T3-E1 cultured on the samples and stained with calcein and propidium iodide on day 10: a) & d) HA-on-chip (perfused at 8 µl/min flow), b) & e) HA-static and c) & f) PS-static. Two different magnifications are displayed.

pability of the non-stoichiometric HA lattice to sustain a variety of cationic and anionic substitutions [9,37]. Specifically, both the uptake of calcium from and release of phosphates into cell culture medium leads to the maturation of the non-stoichiometric HA ($Ca_9(HPO_4)(PO_4)_5(OH)$) towards a more stoichiometric composition ($Ca_{10}(PO_4)_6(OH)_2$). The decrease in HA reactivity observed over time by a slightly lower calcium uptake and a decreased release of phosphate seemed to confirm this maturation. The release of phosphates could be explained by the replacement of these groups by carbonates (B substitution) [38]. However, a complete understanding of the underlying mechanisms behind this ionic exchange would require monitoring of all ionic species in the immersion medium, which was beyond the scope of this work. The characterization of the HA crystal structures before and after contact with cell culture medium for 10 days, either by immersion (HA static) or by flow (HA-on-chip), indicated that while the morphology of the plate-like crystals was not affected (Fig. S.M. 5), the Ca/P ratio experienced a slight increase when compared to 10-day pristine samples (Fig. S.M. 6). These results correlated well with the maturation of HA in biological fluids and were similarly described before [34]. Finally, the cells *per se* did not modify the $[Ca^{2+}]$ and $[P^{5+}]$ levels, as PS-static samples exhibited similar ion concentrations compared to fresh medium levels over a 10-day period (Fig. S.M. 7, and Tables S.M. 2 and S.M. 3).

Since it is known that ionic changes in culture medium can influence the cellular response to the material [8,39], HA-on-chip samples were perfused at three different flow rates to create a range of $[Ca^{2+}]$ and $[P^{5+}]$ that would enable investigation of the biological implications. In the HA-on-chip samples, $[Ca^{2+}]$ and $[P^{5+}]$ in the medium consistently approached levels closer to those found in fresh medium when higher flow rates were applied (Fig. 2). The continuous perfusion influenced the ionic con-

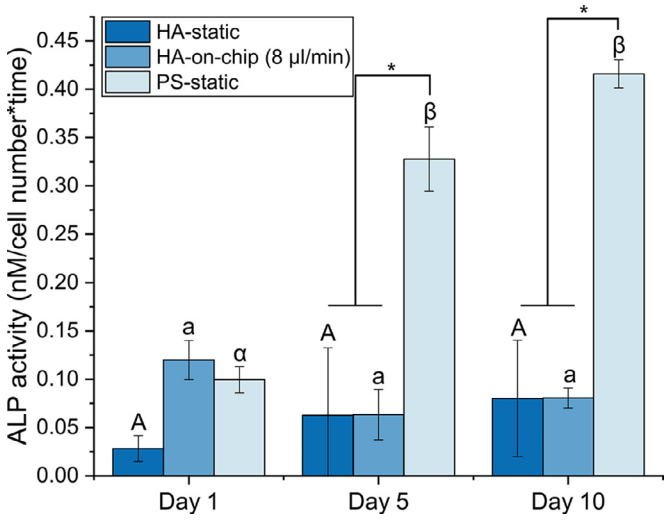

Fig. 6. Cell differentiation expressed as p-nitrophenol concentration (nM) normalized against cell number and reaction time (min). Identical letters between samples of the same type at different time points indicate no statistical significance. * indicates statistical difference between sample types at the same time-point ($p < 0.05$, Post-hoc Tukey).

centration in the medium in two different manners: i) shortening the available time for HA and the medium to establish a chemical equilibrium and ii) shielding the changes in ionic concentration due to a higher volume of medium being in contact with a particular surface area of HA. Specifically, every 24 h, a total volume of 2.8, 11.5 and 20.2 ml was perfused through the HA-on-chip maintained at a flow of 2, 8 and 14 µl/min, respectively, in comparison to 0.2 ml present in the well plate in HA-static samples.

The lower number of adhered MC3T3-E1 cells at 6 h and 72 h on HA-static may be directly related to the decreased [Ca^{2+}] in the medium in comparison to HA-on-chip (Fig. 3). Specifically, the [Ca^{2+}] in the HA-static was 0.8 ± 0.1 mM, this being half the concentration of fresh medium and lower than the [Ca^{2+}] range of 1.0–1.4 mM in HA-on-chip samples (Fig. 2). Although the low internal volume of the HA-on-chip-static samples did not allow measurement of their ionic concentrations, the calcium concentration was possibly even lower than that of HA-static due to a 4-fold higher surface area-to-volume ratio (*i.e.* SA/V; SA/V of HA-on-chip = 17.7 cm^2/ml and SA/V of HA-static = 4.7 cm^2/ml). Such a low concentration of calcium could have led to the death and washout of all seeded cells (Fig. 3A). Therefore, the use of HA-on-chip-static in further analysis of proliferation and differentiation was discontinued.

Calcium is a vital signalling molecule with roles in transcription and motility [40]. The [Ca^{2+}] can be recognized by extracellular calcium receptors of osteoblasts [41] and thus affect cell behaviour. For example, cell adhesion, which is facilitated by transmembrane receptors such as integrins, is jeopardized at low [Ca^{2+}], since this ion is needed to promote the active conformation of the integrin [42]. Dvorak et al. reported a decrease in proliferation of fetal rat calvarial cells at calcium concentrations of 0.5 mM, as compared to fresh medium (calcium concentration of 1.2 mM) [43]. These results could specifically be related to a decreased activation of extracellular signal-regulated kinases (ERK) [44]. In addition, calcium has been observed to be important in cyclo-oxygenase (COX-2) upregulation and prostaglandin-2 (PGE-2) production [45], as well as being involved in Transforming growth factor-β1 (TGF-β1) mediated signalling cascades [46]. Interestingly however, Gustavsson et al. reported that proliferation remained intact in Saos-2 (osteosarcoma osteoblast-like cell line) cells grown in indirect culture with HA despite a calcium level reduction to 0.2 mM during culture, though delays in other osteoblast functions such as differentiation and mineralization were reported [8]. In our work however, MC3T3-E1 cells were cultured directly on the material, with the two factors of direct material contact and a different cell type potentially amplifying the negative response in terms of proliferation observed in HA-static samples. In fact, a previous study culturing MC3T3-E1 on different biomaterials concluded that the low cell viability observed for two calcium phosphate materials (brushite and monetite) in comparison to titanium along a 12-day study was due to the ability of brushite and monetite to absorb calcium ions from the medium [47]. This indicates that MC3T3-E1 cells are particularly sensitive to calcium concentrations in the medium, with low values affecting their proliferation and function.

Similarly to calcium, phosphate has also been reported to be involved in a multitude of cell functions such as cell adhesion, gene expression and protein regulation [48,49]. In HA-on-chip samples, phosphate levels were maintained between 1.1 and 1.4 mM, while levels in HA-static samples peaked at approximately 2.0 ± 0.1 mM, with the concentration in fresh medium being 1.0 ± 0.01 mM (Fig. 2). Adams et al. indicated that high levels of extracellular phosphate (specifically greater than 3 mM) can potentially result in rapid osteoblast apoptosis, with potentially 80% of the cellular population being affected after 6 h of exposure [50]. This behaviour was ascribed to a loss of mitochondrial membrane potential [51] and could lead to the observed lower number of cells attached to the HA surface. Therefore, it is important to keep both calcium and phosphate concentrations within the physiological range in order to ensure an appropriate cell response.

Regarding the influence of different flow rates on MC3T3-E1 proliferation, the results indicated a maximal proliferation at 2 and 8 µl/min, with a slight reduction at 14 µl/min (Fig. 3). Considering the inverse relationship between flow rate magnitude and the modification of ionic concentrations of the medium, the results were surprising since the lowest HA-on-chip degree of proliferation was found at a flow of 14 µl/min, where calcium and phosphate levels were closest to that of fresh medium. This may indicate that it is not possible to ascribe the cell behaviour only to ionic concentrations as other parameters within the microfluidic platform might also impose an effect, such as shear stress and potential washout of signalling molecules.

A flow rate of 8 µl/min was selected when culturing the cells for a longer time period as it provided a high degree of proliferation after 3 days (Fig. 3), while also maintaining concentrations of calcium and phosphate close to that of fresh medium (Fig. 2). In addition, the highest flow rate (14 µl/min) was not considered for further analysis due to practical reasons, as it implies an even higher consumption rate of culture medium. The steady cell proliferation observed in HA-on-chip samples, up to 10 days, indicated that flow continued to exert a positive effect on cell growth, as opposed to HA-static cultures, which showed lower cell counts (Fig. 5). The combination of continuous nutrient supply and waste removal via flow [52], as well as the shielded ionic exchange appeared important for MC3T3-E1 pre-osteoblasts, which are reportedly sensitive to changes in ionic concentration [47].

The shear stress induced within the HA-on-chip maintained at 8 μl/min was 8 × 10^{-3} dyn/cm^2 (Table 1). While this value was calculated using the flow rate set to the pump, in reality it fluctuates in an oscillatory manner due to the mechanical nature of a peristaltic pump (Fig. S.M. 8). The interstitial flow within the bone is due to a combination of vasculature-induced flow, as well as mechanical load on the bone matrix [13,53]. Mathematical models have estimated peak shear stresses on the interior osteon canal surface (where osteoblasts are located) to be between 0.3 and 25 dyn/cm^2 [53]. Another work has estimated the fluid velocity in the LCN to be 24–84 µm/s for mechanically loaded bone [54]. It is important to note that the quoted values reflect con-

ditions in the cytoplasmic processes within the lacuna-canalicular network (LCN). While gap junctions between osteoblastic and osteocyte processes are found in this region [55], the main bulk of the osteoblast cell body is located outside of the LCN, such as on the Haversian canal surface. Due to the Haversian canal being 1000 times larger than the LCN [56], shear stress and fluid velocity on the Haversian canal surface are expected to be notably lower than those in the LCN region [14]. Since a biomaterial can be implanted in different areas of bone, the selection of shear stress and fluid velocity to characterise a biomaterial is challenging. The shear stress and fluid velocity utilised in our microfluidic cell culture (8×10^{-3} dyn/cm^2 and 89 µm/s, respectively) were probably not an exact representation of the physiological conditions, as the flow rate (8 μl/min) was primarily selected to shield against the ionic exchange between HA and medium. In the future, modifications of the microfluidic channel height and width could allow a more thorough reproduction of the physiological conditions in a particular implantation site.

Although the main purpose of the flow profile was not to stimulate the cells directly, the intrinsic shear stress could have influenced osteoblast proliferation. For instance, shear stresses within the range of 1.5–7.7 $\times$ 10^{-5} dyn/cm^2 applied continuously for 24 h in a MC3T3-E1 culture [18] promoted proliferation, while shear stresses above 4.1 $\times$ 10^{-3} dyn/cm^2 inhibited it [18]. Within the same range of stimulation, intermittent shear-stress of 26.6 $\times$ 10^{-5} dyn/cm^2 over 1 h in a human osteoblast culture [57] also caused proliferation. Even stimulating human primary osteoblasts with a higher shear stress of 20 dyn/cm^2 for 30 min appeared to promote proliferation [16]. Similarly, applying a shear stimulus of 17–20 dyn/cm^2 on SaoS-2 osteoblasts for 3 h led to an increase in TGF-β1 expression [19]. Overall, the literature indicates that shear stresses within a wide range can influence cell proliferation but it is difficult to compare to our results due to a number of factors, including usage of different cell types, different shear stress magnitudes and exposure times, as well as the presence of a bioactive material as a cell culture substrate instead of an inert surface.

When examining ALP activity, both HA-on-chip and HA-static showed a low degree of ALP activity compared to the positive control (Fig. 6). Considering HA-static samples, this was potentially due to depleted [Ca^{2+}] (Fig. 4) in accordance with previous work that indicated that [Ca^{2+}] below 1.2 mM lead to a significant decrease in ALP activity [43]. As for HA-on-chip, low ALP signal could potentially be ascribed to the continuous flow applied (8 µl/min), which may prevent the accumulation of extracellular signalling molecules such as prostaglandin [45,58] and nitric oxide [17]. In a previous study, MC3T3-E1 cultured within an *ex vivo* human trabecular bone scaffold for 7 days under a continuous perfusion (10 µl/min) also displayed a low degree of ALP expression [59]. There are different strategies to enable extracellular molecule build-up in microfluidic systems, including medium re-circulation, the use of an extremely low flow rate or the application of flow for only short periods. When working with bioactive biomaterials such as HA, medium re-circulation and periodic flow should be carefully designed to ensure that ion exchange remains shielded throughout the culture period.

In this work, HA was incorporated in a microfluidic chip, with the aim to recreate the dynamic nature of interstitial fluid, which involves ionic exchange shielding and application of shear-stress. The platform significantly increased osteoblast cell proliferation on HA in comparison to static cell culture, indicating the crucial importance of careful design of cell culture systems. In the future, we aim to further expand the evaluation of the HA-on-chip platform using a more representative cell type such as human mesenchymal stem cells, and investigate other relevant parameters such as gene expression and immunofluorescence of key markers (*e.g.* OCN, OPN, ALP and RUNX-2), as well as collagen secretion and formation of calcium deposits.

5. Conclusion

It has recently been reported that there is a lack of correlation between *in vitro* and *in vivo* assays of biomaterials for bone applications. In the case of bioactive biomaterials as calcium-deficient hydroxyapatite (HA), an explanation may be the prompt calcium uptake and phosphate release that is observed when a material is immersed in cell culture medium. In order to improve the *in vitro* cell culture environment, HA was integrated in a microfluidic chip (designated as HA-on-chip). The higher flow rates (within a 2−14 µl/min range) applied in the HA-on-chip resulted in calcium and phosphate concentrations closer to those of fresh medium. Moreover, cells cultured on HA-on-chip showed a higher degree of proliferation than cells cultured on HA in static conditions, which was ascribed to shielded ion exchange, as well as to improved nutrient supply and waste removal. However, ALP activity was low in both HA-on-chip and HA-static samples, with a depletion of signalling molecules and low calcium levels being proposed as potential explanations for each, respectively. This study indicates the importance of the *in vitro* methodology chosen to evaluate the biological properties of biomaterials, raising awareness of the importance of using methods that better approach the physiological conditions.

Declaration of Competing Interest

A.R. Atif, M. Pujari-Palmer, M. Tenje and G. Mestres declare that they have no conflicts of interest.

Acknowledgements

The authors would also like to thank Adam Engberg and David Wenner for their assistance with 3D printing the moulds and fabricating the α-TCP powder, respectively. The authors would also like to acknowledge Håkan Engqvist for scientific support. GM acknowledges the Swedish Council Formas (#2016-00781), Swedish Council Vetenskapsrådet (#2017-05051) and Göran Gustafsson's Foundation (#1841) for funding this research. MT acknowledges funding from the Knut and Alice Wallenberg Foundation (#2016-0112).

Supplementary materials

Supplementary material associated with this article can be found, in the online version, at doi:10.1016/j.actbio.2021.03.046.

References

[1] R.A. Perez, G. Mestres, Role of pore size and morphology in musculo-skeletal tissue regeneration, Mater. Sci. Eng. C Mater. Biol. Appl. 61 (2016) 922–939, doi:10.1016/j.msec.2015.12.087.
[2] K. Anselme, M. Bigerelle, Role of materials surface topography on mammalian cell response, Int. Mater. Rev. 56 (2011) 243–266, doi:10.1179/1743280411Y.0000000001.
[3] G. Hulsart-Billström, J.I. Dawson, S. Hofmann, R. Müller, M.J. Stoddart, M. Alini, H. Redl, A. El Haj, R. Brown, V. Salih, J. Hilborn, S. Larsson, R.O. Oreffo, A surprisingly poor correlation between in vitro and in vivo testing of biomaterials for bone regeneration: results of a multicentre analysis, Eur. Cell. Mater. 31 (2016) 312–322, doi:10.22203/eCM.v031a20.
[4] G. Mestres, R.A. Perez, N.L. D'Elía, L. Barbe, Advantages of microfluidic systems for studying cell-biomaterial interactions-focus on bone regeneration applications, Biomed. Phys. Eng. Express 5 (2019) 032001, doi:10.1088/2057-1976/ab1033.
[5] M.-P. Ginebra, M. Espanol, Y. Maazouz, V. Bergez, D. Pastorino, Bioceramics and bone healing, EFORT Open Rev. 3 (2018) 173–183, doi:10.1302/2058-5241.3.170056.
[6] G. Mestres, M. Espanol, W. Xia, C. Persson, M.-P. Ginebra, M.K. Ott, Inflammatory response to nano- and microstructured hydroxyapatite, PLOS One 10 (2015) e0120381, doi:10.1371/journal.pone.0120381.

[7] J.-M. Sadowska, J. Guillem-Marti, E.B. Montufar, M. Espanol, M.-P. Ginebra, Biomimetic versus sintered calcium phosphates: the in vitro behavior of osteoblasts and mesenchymal stem cells, Tissue Eng. Part A 23 (2017) 1297–1309, doi:10.1089/ten.tea.2016.0406.
[8] J. Gustavsson, M.P. Ginebra, J. Planell, E. Engel, Osteoblast-like cellular response to dynamic changes in the ionic extracellular environment produced by calcium-deficient hydroxyapatite, J. Mater. Sci. Mater. Med. 23 (2012) 2509–2520, doi:10.1007/s10856-012-4705-4.
[9] J. Gustavsson, M.P. Ginebra, E. Engel, J. Planell, Ion reactivity of calcium-deficient hydroxyapatite in standard cell culture media, Acta Biomater. 7 (2011) 4242–4252, doi:10.1016/j.actbio.2011.07.016.
[10] S. Maeno, Y. Niki, H. Matsumoto, H. Morioka, T. Yatabe, A. Funayama, Y. Toyama, T. Taguchi, J. Tanaka, The effect of calcium ion concentration on osteoblast viability, proliferation and differentiation in monolayer and 3D culture, Biomaterials 26 (2005) 4847–4855, doi:10.1016/j.biomaterials.2005.01.006.
[11] M.L.K. Tate, R. Steck, M.R. Forwood, P. Niederer, In vivo demonstration of load--induced fluid flow in the rat tibia and its potential implications for processes associated with functional adaptation, J. Exp. Biol. 203 (2000) 2737–2745.
[12] S.C. Cowin, L. Cardoso, Blood and Interstitial flow in the hierarchical pore space architecture of bone tissue, J. Biomech. 48 (2015) 842–854, doi:10.1016/j.jbiomech.2014.12.013.
[13] J. Rubin, C. Rubin, C.R. Jacobs, Molecular pathways mediating mechanical signaling in bone, Gene 367 (2006) 1–16, doi:10.1016/j.gene.2005.10.028.
[14] E.H. Burger, J. Klein-Nulend, Mechanotransduction in bone-role of the lacuno-canalicular network, FASEB J. 13 (1999) S101–S112, doi:10.1096/fasebj.13.9001.s101.
[15] P.S. Vezeridis, C.M. Semeins, Q. Chen, J. Klein-Nulend, Osteocytes subjected to pulsating fluid flow regulate osteoblast proliferation and differentiation, Biochem. Biophys. Res. Commun. 348 (2006) 1082–1088, doi:10.1016/j.bbrc.2006.07.146.
[16] S. Kapur, D.J. Baylink, K.-H.William Lau, Fluid flow shear stress stimulates human osteoblast proliferation and differentiation through multiple interacting and competing signal transduction pathways, Bone 32 (2003) 241–251, doi:10.1016/S8756-3282(02)00979-1.
[17] D.L. Johnson, T.N. McAllister, J.A. Frangos, Fluid flow stimulates rapid and continuous release of nitric oxide in osteoblasts, Am. J. Physiol. 271 (1996) E205–E208, doi:10.1152/ajpendo.1996.271.1.E205.
[18] W. Yu, H. Qu, G. Hu, Q. Zhang, K. Song, H. Guan, T. Liu, J. Qin, A microfluidic-based multi-shear device for investigating the effects of low fluid-induced stresses on osteoblasts, PloS One 9 (2014) e89966, doi:10.1371/journal.pone.0089966.
[19] K. Sakai, M. Mohtai, Y. Iwamoto, Fluid Shear stress increases transforming growth factor beta 1 expression in human osteoblast-like cells: modulation by cation channel blockades, Calcif. Tissue Int. 63 (1998) 515–520, doi:10.1007/s002239900567.
[20] A. Hoppe, N.S. Güldal, A.R. Boccaccini, A review of the biological response to ionic dissolution products from bioactive glasses and glass-ceramics, Biomaterials 32 (2011) 2757–2774, doi:10.1016/j.biomaterials.2011.01.004.
[21] J.S. Stephens, J.A. Cooper, F.R. Phelan, J.P. Dunkers, Perfusion flow bioreactor for 3D in situ imaging: Investigating cell/biomaterials interactions, Biotechnol. Bioeng. 97 (2007) 952–961, doi:10.1002/bit.21252.
[22] A. Hartmann, M. Stamp, R. Kmeth, S. Buchegger, B. Stritzker, B. Saldamli, R. Burgkart, M.F. Schneider, A. Wixforth, A novel tool for dynamic cell adhesion studies–the de-adhesion number investigator DANI, Lab. Chip. 14 (2013) 542–546, doi:10.1039/C3LC50916H.
[23] M.E.M. Stamp, A.M. Jötten, P.W. Kudella, D. Breyer, F.G. Strobl, T.M. Geislinger, A. Wixforth, C. Westerhausen, Exploring the limits of cell adhesion under shear stress within physiological conditions and beyond on a chip, Diagn. Basel Switz. 6 (2016), doi:10.3390/diagnostics6040038.
[24] J.-H. Lee, Y. Gu, H. Wang, W.Y. Lee, Microfluidic 3D bone tissue model for high-throughput evaluation of wound-healing and infection-preventing biomaterials, Biomaterials 33 (2012) 999–1006, doi:10.1016/j.biomaterials.2011.10.036.
[25] S.-S.D. Carter, L. Barbe, M. Tenje, G. Mestres, Exploring microfluidics as a tool to evaluate the biological properties of a titanium alloy under dynamic conditions, Biomater. Sci. (2020), doi:10.1039/D0BM00964D.
[26] H. Bahmaee, R. Owen, L. Boyle, C.M. Perrault, A.A. Garcia-Granada, G.C. Reilly, F. Claeyssens, Design and evaluation of an osteogenesis-on-a-chip microfluidic device incorporating 3D cell culture, Front. Bioeng. Biotechnol. 8 (2020), doi:10.3389/fbioe.2020.557111.
[27] N. Jusoh, S. Oh, S. Kim, J. Kim, N.L. Jeon, Microfluidic vascularized bone tissue model with hydroxyapatite-incorporated extracellular matrix, Lab. Chip. 15 (2015) 3984–3988, doi:10.1039/C5LC00698H.
[28] Q. Tang, X. Li, C. Lai, L. Li, H. Wu, Y. Wang, X. Shi, Fabrication of a hydroxyapatite-PDMS microfluidic chip for bone-related cell culture and drug screening, Bioact. Mater. 6 (2021) 169–178, doi:10.1016/j.bioactmat.2020.07.016.
[29] W.N. Addison, V. Nelea, F. Chicatun, Y.-C. Chien, N. Tran-Khanh, M.D. Buschmann, S.N. Nazhat, M.T. Kaartinen, H. Vali, M.M. Tecklenburg, R.T. Franceschi, M.D. McKee, Extracellular matrix mineralization in murine MC3T3-E1 osteoblast cultures: an ultrastructural, compositional and comparative analysis with mouse bone, Bone 71 (2015) 244–256, doi:10.1016/j.bone.2014.11.003.
[30] D. Wang, K. Christensen, K. Chawla, G. Xiao, P.H. Krebsbach, R.T. Franceschi, Isolation and characterization of MC3T3-E1 preosteoblast subclones with distinct in vitro and in vivo differentiation/mineralization potential, J. Bone Miner. Res. Off. J. Am. Soc. Bone Miner. Res. 14 (1999) 893–903, doi:10.1359/jbmr.1999.14.6.893.
[31] C.-L.E. Helm, M.E. Fleury, A.H. Zisch, F. Boschetti, M.A. Swartz, Synergy between interstitial flow and VEGF directs capillary morphogenesis in vitro through a gradient amplification mechanism, Proc. Natl. Acad. Sci. 102 (2005) 15779–15784, doi:10.1073/pnas.0503681102.
[32] J. Schindelin, I. Arganda-Carreras, E. Frise, V. Kaynig, M. Longair, T. Pietzsch, S. Preibisch, C. Rueden, S. Saalfeld, B. Schmid, J.-Y. Tinevez, D.J. White, V. Hartenstein, K. Eliceiri, P. Tomancak, A. Cardona, Fiji: an open-source platform for biological-image analysis, Nat. Methods 9 (2012) 676–682, doi:10.1038/nmeth.2019.
[33] K. Klimek, A. Belcarz, R. Pazik, P. Sobierajska, T. Han, R.J. Wiglusz, G. Ginalska, False" cytotoxicity of ions-adsorbing hydroxyapatite–corrected method of cytotoxicity evaluation for ceramics of high specific surface area, Mater. Sci. Eng. C 65 (2016) 70–79, doi:10.1016/j.msec.2016.03.105.
[34] J.M. Sadowska, J. Guillem-Marti, M. Espanol, C. Stähli, N. Döbelin, M.-P. Ginebra, In vitro response of mesenchymal stem cells to biomimetic hydroxyapatite substrates: A new strategy to assess the effect of ion exchange, Acta Biomater. 76 (2018) 319–332, doi:10.1016/j.actbio.2018.06.025.
[35] R. Olkowski, P. Kaszczewski, J. Czechowska, D. Siek, D. Pijocha, A. Zima, A. Ślósarczyk, M. Lewandowska-Szumieł, Cytocompatibility of the selected calcium phosphate based bone cements: comparative study in human cell culture, J. Mater. Sci. Mater. Med. (2015) 26, doi:10.1007/s10856-015-5589-x.
[36] S. Hao, L. Ha, G. Cheng, Y. Wan, Y. Xia, D.M. Sosnoski, A.M. Mastro, S.-Y. Zheng, A spontaneous 3D bone-on-a-chip for bone metastasis study of breast cancer cells, Small 14 (2018) 1702787, doi:10.1002/smll.201702787.
[37] S.V. Dorozhkin, M. Epple, Biological and medical significance of calcium phosphates, Angew. Chem. Int. Ed. 41 (2002) 3130–3146, doi:10.1002/1521-3773(20020902)41:17⟨3130::AID-ANIE3130⟩3.0.CO;2-1.
[38] E. Boanini, M. Gazzano, A. Bigi, Ionic substitutions in calcium phosphates synthesized at low temperature, Acta Biomater. 6 (2010) 1882–1894, doi:10.1016/j.actbio.2009.12.041.
[39] Y.C. Chai, S.J. Roberts, J. Schrooten, F.P. Luyten, Probing the osteoinductive effect of calcium phosphate by using an in vitro biomimetic model, Tissue Eng. Part A 17 (2010) 1083–1097, doi:10.1089/ten.tea.2010.0160.
[40] D.E. Clapham, Calcium signaling, Cell 131 (2007) 1047–1058, doi:10.1016/j.cell.2007.11.028.
[41] N. Chattopadhyay, S. Yano, J. Tfelt-Hansen, P. Rooney, D. Kanuparthi, S. Bandyopadhyay, X. Ren, E. Terwilliger, E.M. Brown, Mitogenic action of calcium-sensing receptor on rat calvarial osteoblasts, Endocrinology 145 (2004) 3451–3462, doi:10.1210/en.2003-1127.
[42] A.P. Mould, A.N. Garratt, W. Puzon-McLaughlin, Y. Takada, M.J. Humphries, Regulation of integrin function: evidence that bivalent-cation-induced conformational changes lead to the unmasking of ligand-binding sites within integrin alpha5 beta1, Biochem. J. 331 (1998) 821–828, doi:10.1042/bj3310821.
[43] M.M. Dvorak, A. Siddiqua, D.T. Ward, D.H. Carter, S.L. Dallas, E.F. Nemeth, D. Riccardi, Physiological changes in extracellular calcium concentration directly control osteoblast function in the absence of calciotropic hormones, Proc. Natl. Acad. Sci. USA 101 (2004) 5140–5145, doi:10.1073/pnas.0306141101.
[44] Z. Huang, S.L. Cheng, E. Slatopolsky, Sustained activation of the extracellular signal-regulated kinase pathway is required for extracellular calcium stimulation of human osteoblast proliferation, J. Biol. Chem. 276 (2001) 21351–21358, doi:10.1074/jbc.M010921200.
[45] S. Choudhary, S. Wadhwa, L.G. Raisz, C. Alander, C.C. Pilbeam, Extracellular calcium is a potent inducer of cyclo-oxygenase-2 in murine osteoblasts through an ERK signaling pathway, J. Bone Miner. Res. Off. J. Am. Soc. Bone Miner. Res. 18 (2003) 1813–1824, doi:10.1359/jbmr.2003.18.10.1813.
[46] L.J. Nesti, E.J. Caterson, W.-J. Li, R. Chang, T.D. McCann, J.B. Hoek, R.S. Tuan, TGF- 1 calcium signaling in osteoblasts, J. Cell. Biochem. 101 (2007) 348–359, doi:10.1002/jcb.21180.
[47] U. Klammert, T. Reuther, C. Jahn, B. Kraski, A.C. Kübler, U. Gbureck, Cytocompatibility of brushite and monetite cell culture scaffolds made by three-dimensional powder printing, Acta Biomater. 5 (2009) 727–734, doi:10.1016/j.actbio.2008.08.019.
[48] G.R. Beck, B. Zerler, E. Moran, Phosphate is a specific signal for induction of osteopontin gene expression, Proc. Natl. Acad. Sci. 97 (2000) 8352–8357, doi:10.1073/pnas.140021997.
[49] T. Michigami, M. Kawai, M. Yamazaki, K. Ozono, Phosphate as a signaling molecule and its sensing mechanism, Physiol. Rev. 98 (2018) 2317–2348, doi:10.1152/physrev.00022.2017.
[50] C.S. Adams, K. Mansfield, R.L. Perlot, I.M. Shapiro, Matrix regulation of skeletal cell apoptosis. Role of calcium and phosphate ions, J. Biol. Chem. 276 (2001) 20316–20322, doi:10.1074/jbc.M006492200.
[51] Z. Meleti, I.M. Shapiro, C.S. Adams, Inorganic phosphate induces apoptosis of osteoblast-like cells in culture, Bone 27 (2000) 359–366, doi:10.1016/S8756-3282(00)00346-X.
[52] M. Tehranirokh, A.Z. Kouzani, P.S. Francis, J.R. Kanwar, Microfluidic devices for cell cultivation and proliferation, Biomicrofluidics 7 (2013) 051502, doi:10.1063/1.4826935.
[53] L. Wang, S.P. Fritton, S. Weinbaum, S.C. Cowin, On bone adaptation due to venous stasis, J. Biomech. 36 (2003) 1439–1451.
[54] C. Price, X. Zhou, W. Li, L. Wang, Real-time measurement of solute transport within the lacunar-canalicular system of mechanically loaded bone: direct evidence for load-induced fluid flow, J. Bone Miner. Res. 26 (2011) 277–285, doi:10.1002/jbmr.211.

[55] J.P. Stains, R. Civitelli, Gap junctions in skeletal development and function, Biochim. Biophys. Acta BBA–Biomembr. 1719 (2005) 69–81, doi:10.1016/j.bbamem.2005.10.012.
[56] V.I. Sikavitsas, J.S. Temenoff, A.G. Mikos, Biomaterials and bone mechanotransduction, Biomaterials 22 (2001) 2581–2593, doi:10.1016/s0142-9612(01)00002-3.
[57] U.M. Liegibel, U. Sommer, B. Bundschuh, B. Schweizer, U. Hilscher, A. Lieder, P. Nawroth, C. Kasperk, Fluid shear of low magnitude increases growth and expression of TGF 1 and adhesion molecules in human bone cells in vitro, Exp. Clin. Endocrinol. Diabetes 112 (2004) 356–363, doi:10.1055/s-2004-821014.
[58] D.C. Genetos, D.J. Geist, D. Liu, H.J. Donahue, R.L. Duncan, Fluid shear-induced ATP secretion mediates prostaglandin release in MC3T3-E1 osteoblasts, J. Bone Miner. Res. 20 (2005) 41–49, doi:10.1359/JBMR.041009.
[59] S.H. Cartmell, B.D. Porter, A.J. García, R.E. Guldberg, Effects of medium perfusion rate on cell-seeded three-dimensional bone constructs in vitro, Tissue Eng. 9 (2003) 1197–1203, doi:10.1089/10763270360728107.